https://doi.org/10.20965/jrm.2020.p1061

Paper:

Design and Modeling of Soft Pneumatic Helical Actuator with High Contraction Ratio

Peizheng Yuan, Ginjiro Kawano, and Hideyuki Tsukagoshi

Tokyo Institute of Technology
2-12-1 Ookayama, Meguro-ku, Tokyo 152-8552, Japan
[Received May 20, 2020; accepted August 18, 2020]

Soft contraction actuators are becoming important elements particularly for human-friendly robotic applications. However, it is challenging to achieve both a large operating distance while generating practical force. Hence, we present a new soft contraction actuator capable of realizing a high ratio contraction by pneumatic power. It can be easily fabricated using soft materials, including rubber tubes, one-way extensible cloth, and inextensible wire. Its initial shape is tubular but it can curve and coil to a helix shape owing to its different extensibilities on two sides when pressurized. A maximum contraction ratio of 78% and a 23 N contraction force can be achieved with an 11.6 mm initial outer diameter tube under 0.3 MPa. The effect of the tilt angle of a one-way extensible cloth on the helical shape is investigated, and a mathematical model illustrating the relationship between the contraction ratio and force is derived. Our experimental results suggest that this helical actuator has a much higher contraction ratio than a McKibben actuator under the same conditions. Finally, we discuss the potential application of the proposed actuator to a wearable device, i.e., for assisting the dorsiflexion of an ankle joint requiring a wide range of motion.

Keywords: pneumatics, soft actuator, wearable robot

1. Introduction

Soft robots have been rapidly developed owing to their high adaptability to different environments and their ability to realize safe and compliant interactions with target objects [1]. For example, various studies have been conducted in terms of rehabilitation because soft wearable robot devices have high affinity with the human body [2–5]. Soft exosuits were developed for walking support [6]. Hand rehabilitation [7] soft robot splint was developed for wrist rehabilitation [8], and cases of applying a pneumatic soft rubber actuator to the backbone have been reported [9].

Soft contraction actuators are an important research branch in soft robotics, some of which are known as pneumatic artificial muscles (PAMs) as they have the same operating performance as human muscles. PAMs can realize controllable contraction and controllable torque by controlling the air pressure inside the actuator chamber [10]; hence, it can be widely used in bionics research, medical rehabilitation, and other areas where soft interaction and contraction are both required. The McKibben pneumatic actuator was invented in the 1950s. Although it can produce a considerable contraction force along its tubular body, the contraction ratio is low, typically less than 30% [11]. Some contraction actuators use soft bellows and can only realize a high contraction ratio by applying a negative pressure to the internal chamber, such as the agonistic pneumatic artificial muscle [12] and vacuum bellows actuator [13]. However, actuators driven by negative pressures have inherent pressure limitations; therefore, their controllable pressure ranges become smaller. Helical actuators have been developed, and some of them are only designed for expanding [14] or for grasping objects [15]. However, some others have a contraction function because they do not use extensible materials [16] or allow the actuator to operate initially in a helical shape [17]; hence, their contraction ratio remains low. Therefore, the design of a simple structure to realize a high contraction ratio (greater than 50%) under a positive air pressure remains a problem in soft robotics.

To address this problem, the authors proposed a soft pneumatic helical actuator (**Fig. 1**) that generates a 78% contraction rate, of which its operating principle and fabrication method are available in [18]. In this study, we constructed a mathematical model of our previous actuator to validate it by demonstrating the relationship between its displacement and force. In addition, as a proposed application of the actuator, we present an example of an ankle support device and analyze its effectiveness.

2. Actuator Design and Driving Principles

2.1. Structure and Fabrication

A one-way extensible cloth is a specially fabricated cloth with perpendicularly braided elastic string and nonstretchable fiber such that only one direction is extensible but the perpendicular direction is inextensible. When a sleeve fabricated using a one-way extensible cloth is used to cover a rubber tube, the angle between the fiber-weaving direction (inextensible direction) and the axial

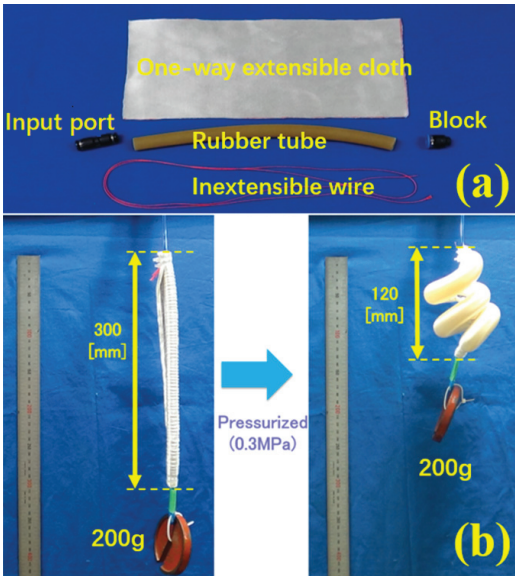

Fig. 1. (a) Helical actuators can be fabricated using simple and cheap materials. (b) Helical actuators can realize 60% contraction ratio with 200 g load under 0.3 MPa.

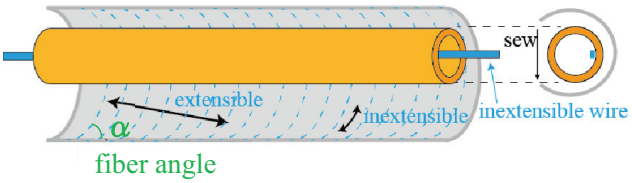

Fig. 2. Structure of helical actuator.

direction of the sleeve will affect the shape of the helix after it is being pressurized. We name this angle the fiber angle of the sleeve. The main structure of the helical actuator and the fiber angle are shown in **Fig. 2**.

Based on its simple structure, the fabrication of a helical actuator can be conducted in the following three steps:

1. Place the inextensible wire inside the tube on one side of the inner surface and place the tube on a piece of a one-way extensible cloth.
2. Sew the cloth into a sleeve along the tube.
3. Fix the inlet and block at the two ends of the tube, and fix the wire, tube, cloth, and inlet (block) together to ensure that the wire is attached on the same side of the inner surface of the tube.

2.2. Driving Principle

First, we assumed that the fiber angle was 90°, signifying that the inextensible fiber inside the cloth was parallel to the circumferential direction of the tube, and the extensible direction was along the axial direction of the tube.

As introduced in the previous section, the rubber tube was covered with a one-way extensible cloth and fixed with an inextensible wire inside it. When pressurized by air, as the air pressure inside the rubber tube increased,

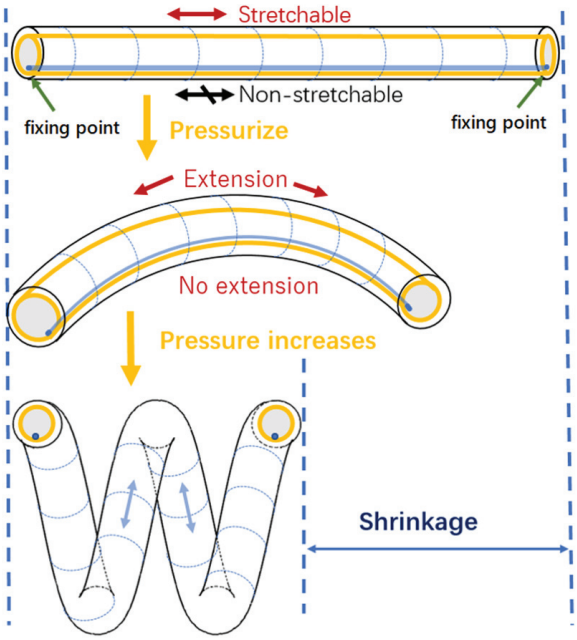

Fig. 3. Driving principle of helical actuator.

the volume of the tube expanded in both the axial and circumferential directions. However, because it was covered by a one-way extensible cloth, the expansion in the circumferential direction was blocked.

Meanwhile, because the cloth was extensible along the axial direction, it did not restrict the expansion of the rubber tube. However, inside the tube, the inextensible wire was attached to one side of the inner surface. Hence, for the rubber tube, most of its parts can expand in the axial direction but only a thin line-shaped part restricted by an inextensible wire cannot; therefore, it maintains its original length before being pressurized. Consequently, the length of the actuator on the two sides will differ; therefore, it will curve and bend toward the direction where the inextensible wire is fixed. In this case, the entire actuator will resemble a curve in a two-dimensional plane.

Next, we consider the case where the fiber angle is less than 90°. In this case, the extensible direction of the cloth will not be strictly along the axial direction of the tube; instead, an acute angle exists between them. Similarly, the inextensible direction of the cloth will yield an acute angle with the circumferential direction of the tube. In this case, when pressurized, the curing and bending motion of the actuator will not be limited to within a two-dimensional plane but to a three-dimensional space; therefore, the actuator will deform into a three-dimensional helix.

Based on the analysis above, we fabricated a helical actuator for the case where the fiber angle is an acute angle. When pressurized, the actuator bends in a three-dimensional space. When the air pressure increases, the length difference between the two sides of the actuator increases, and the actuator will spiral on a larger scale before finally transforming into a helix (**Fig. 3**).

When a traction force is applied at the end of the helical actuator, the helix will first lengthen in the axial direction,

and the tension generated along the extensible direction will produce an axial force component; hence, the actuator can generate a contraction force, as shown in **Fig. 1(b)**.

3. Characteristics

When fabricating the actuator, we discovered that the fiber angle of the extensible cloth affected the shape of the helix when pressurized. In fact, for most soft actuators fabricated using soft weaving materials, the fiber angle or weaving direction will affect the mechanical characteristics of the soft actuator. In some cases, finite element simulations were used to analyze this type of effect [19].

In this study, we experimentally analyzed the relationship between the fiber angle of the extensible cloth and the helical shape after pressurization. In the extensible cloth, the inextensible fiber was weaved vertically to the extensible direction, where the fiber angle α is the angle between the fiber direction and the axial direction of the sleeve. As introduced in the previous section, when the fiber angle is 90°, the extensible direction of the cloth is along the axial direction of the sleeve. However, when we set the fiber angle to less than 90° to create a sleeve, the actuator will deform into a new spiral shape under the same pressure. Because the stretch direction of the rubber tube and the stretch direction of the cloth are inconsistent, a pinch angle will appear along the helical axis; consequently, the axial length and helical radius of the actuator will change.

Generally, the shape of a three-dimensional space curve can be determined by its curvature and torsion. Conventionally, a helical curve in three-dimensional space can be described using the following equation:

$$r(t) = \begin{pmatrix} a\cos t \\ a\sin t \\ bt \end{pmatrix}, \quad \ldots\ldots\ldots\ldots \quad (1)$$

where t is parametric; a is the spiral radius; b is the increasing speed of the curve that is related to the pinch angle θ and helical length x_0 of the actuator. In this case, the curvature κ and torsion τ can be calculated using the following equations:

$$a = \frac{\kappa}{\kappa^2 + \tau^2}, \quad b = \frac{\tau}{\kappa^2 + \tau^2}. \quad \ldots\ldots\ldots \quad (2)$$

Therefore, we obtain

$$\kappa = \frac{a}{a^2 + b^2}, \quad \tau = \frac{b}{a^2 + b^2}. \quad \ldots\ldots\ldots \quad (3)$$

As shown in Eq. (3), both a and b are determined by κ and τ, suggesting that the shape of the spiral can be determined by those two parameters.

When the input air pressure is specified and remains constant, κ and τ are determined by the fiber angle of the extensible cloth. Because a and b are governed by the fiber angle, the helical radius a, pinch angle θ, and axial length x_0 of the actuator will be affected by the fiber angle α, as shown in **Fig. 4**.

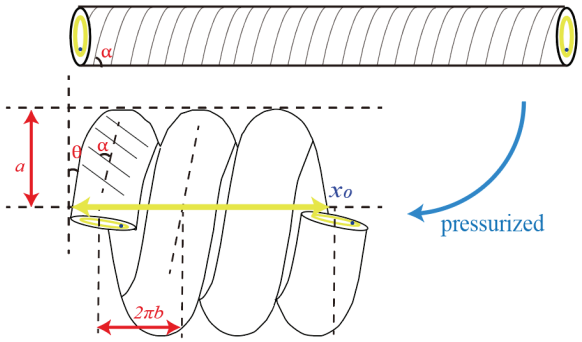

Fig. 4. Fiber angle α governs helical radius and axial length of actuator.

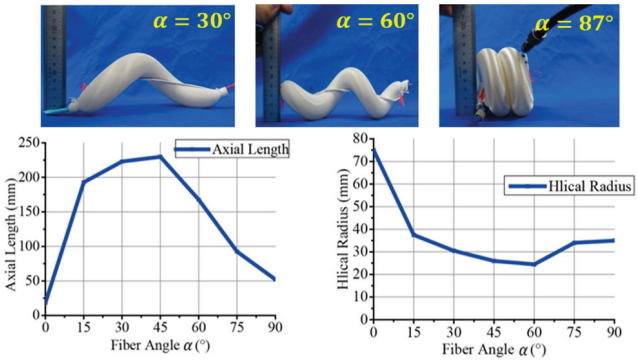

Fig. 5. Experiments revealing relationship between fiber angle and each of axial length and helical radius of one-way extensible cloth.

We conducted experiments to analyze the effect of the fiber angle α on the helical shape: several actuators were fabricated using the same rubber tube (outer diameter = 11.6 mm, length = 200 mm) covered by an extensible cloth with different fiber angles. We recorded the axial length and helical radius for all actuators when they were pressurized by the same air pressure (0.3 MPa).

The results of this experiment are shown in **Fig. 5**. The results show that as the fiber angle α increased from 0° to 90°, the axial length of the actuator increased and then decreased. By contrast, the helical radius decreased and then increased. In certain situations, when $\alpha = 0°$, the actuator can exhibit the largest radius and the shortest axial length. When $\alpha = 45°$, the actuator exhibited the longest and smallest radii. When α approached 87°, the actuator formed a spiral with a short axial length and a relatively small radius, implying that a high contraction ratio and a small radial size can be realized.

Based on the analysis above, we fabricated a helical actuator using an extensible cloth with a fiber angle of 87°. We tested the performance of the helical actuator based on this fiber angle under different loads. The air pressure remained at 0.3 MPa, whereas the loads borne by the actuator included 0, 200, and 500 g. The results are shown in **Fig. 6**. As shown, a maximal contraction ratio of 78% was realized when the load was 0.

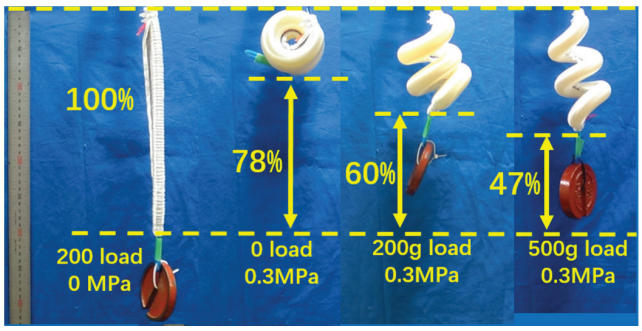

Fig. 6. Different contraction ratios of helical actuator with different loads and same pressure when fiber angle = 87°.

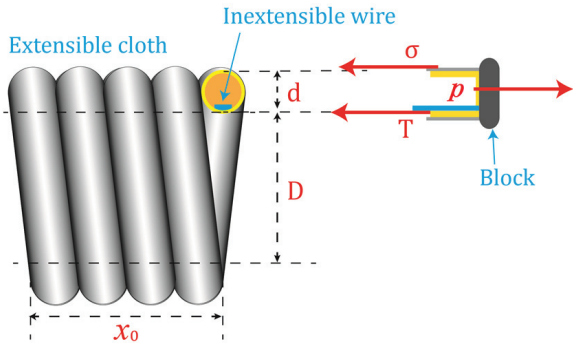

Fig. 7. When pressurized and no outer force is applied, actuator deforms into a helix.

4. Modeling

In this section, the relationship between the contraction force and contraction length of the helical actuator is analyzed. Although studies have been conducted to set a model for a helical actuator, e.g., a kinematic model based on an electroactive polymer that can realize a helical deformation [20] and a model of a artificial muscle derived using a virtual work principle [21], the force characteristics of helical contraction actuators have not been analyzed. Therefore, we derived a model based on the geometric and mechanical analyses of a helical actuator.

To analyze the factors affecting the relationship between contraction force and contraction length, force analysis based on the geometric structure of the helical actuator is necessary. The analysis presented below is based on a helical actuator with a fiber angle of 87° for achieving the best contraction performance. To simplify the discussion in the modeling process, the following were assumed:

1. Assuming that the actuator is placed horizontally, the block of the actuator is on the right side and the inlet on the left side.
2. The traction force is applied horizontally at the center of the block.
3. The fiber angle is 90° for the geometry analysis of the actuator.
4. No acceleration occurs during the contraction process of the actuator.

4.1. Deformation with No Load

When the actuator is pressurized by the input air, the actuator will curve and then deform into a helical shape when no outer force is applied. In this condition, the circumferential tension generated by the radical expansion of the tube and extensible cloth will have all of its tangential directions, which are equal to each other, along the sectional circle of the tube; therefore, they will eliminate each other.

Meanwhile, the axial tension generated by the one-side axial expansion by the tube and the extensible cloth will pull the entire actuator together and compress it into a cylinder containing several layers of coiling tube covered by cloth. They are enforced to attach to each other tightly, resembling a spring (**Fig. 7**). To simplify the model, we assumed no space between each layer.

In this condition, based on the force balance at the block of the actuator, the following equation is obtained:

$$\frac{p\pi d^2}{4} = \sigma + T, \quad \ldots\ldots\ldots\ldots\ldots\ldots \quad (4)$$

where p denotes the air pressure inside the tube, σ the axial tension generated by the tube and cloth, T the traction force of the wire, and d the outer diameter of the tube, which is similar to the inner diameter if the thicknesses of the tube and cloth are negligible.

Considering the forces applied on the block shown in **Fig. 7**, the pressure force was applied on the entire bottom of the block. Additionally, because the bottom was a circle plain, the force can be regarded as being applied at the center of the circle. Whereas σ and T are applied on the opposite sides of the bottom, to ensure that the bottom will not turn around, σ and T should satisfy a torque balance equation. The arm of T can be regarded as $d/2$, but the equivalent application point depends on the curving situation of different parts of the extensible cloth. Considering that the arm of σ should be a multiple of the arm of T, we can assume that it is $k(d/2)$. Subsequently, we obtain the torque balance equation as follows:

$$\sigma \times k\frac{d}{2} = T \times \frac{d}{2}, \quad \ldots\ldots\ldots\ldots\ldots\ldots \quad (5)$$

where k is the ratio between 0 and 1. The tension σ depends on the Young's modulus of the material and the area change. From Eq. (5), we can obtain the relation between σ and T, i.e.,

$$\sigma + T = (1+k)\sigma = (1+k)(E_1 + E_2)\Delta S, \quad \ldots \quad (6)$$

where E_1 and E_2 denote the Young's moduli of the rubber tube and extensible cloth, respectively; ΔS represents the area change of the extensible cloth.

Because no space exists between each layer of the helical shape, the length of the tube after extension can be calculated easily. Suppose L_0 represents the inner length

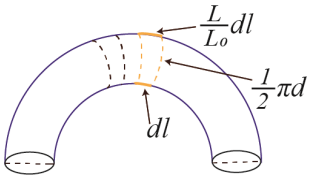

Fig. 8. Calculation method of every small curing area on surface of helical actuator.

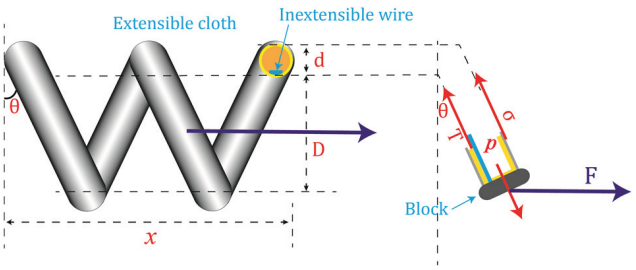

Fig. 9. When actuator is pressurized and traction force is applied, a new force balance is established.

of the actuator because it is constrained by the wire; therefore, L_0 can represent the initial length of the tube, which is known and constant. Suppose L represents the current length of the outer length of the tube x_0 and represents the axial length of the actuator in this situation. Therefore, the following equations can be used to calculate L_0, L, and x_0:

$$L_0 = \pi D n, \quad \ldots \quad (7)$$

$$L = \pi(D+2d)n, \quad \ldots \quad (8)$$

$$x_0 = nd = \frac{L_0 d}{\pi D}, \quad \ldots \quad (9)$$

where n denotes the number of layers of the helix, and D is the inner diameter of the helix.

Subsequently, we can apply calculus to obtain the area change ΔS. If we assume a small length dl along the inner curve of the tube because the outer part of the tube is stretched averagely, the corresponding outer length should be $(L/L_0)dl$ (**Fig. 8**). Using Eqs. (7) and (8), every small curving area of the actuator's surface can be calculated as

$$dS = \frac{1}{2}\left(dl + \frac{L}{L_0}dl\right)\frac{\pi d}{2} = \frac{\pi d}{4}\left(1+\frac{L}{L_0}\right)dl = \frac{\pi d}{2}\left(1+\frac{d}{D}\right)dl. \quad (10)$$

In this case, the current area S can be calculated as follows:

$$S = \int_0^{L_0} 2\,dS = \int_0^{L_0} \pi d\left(1+\frac{d}{D}\right)dl = \pi d L_0\left(1+\frac{d}{D}\right). \quad \ldots \quad (11)$$

Therefore, we can obtain the area change ΔS as follows:

$$\Delta S = S - S_0 = \pi d L_0\left(1+\frac{d}{D}\right) - \pi d L_0 = \frac{\pi d^2 L_0}{D}, \quad \ldots \quad (12)$$

where S_0 represents the initial surface area of the actuator before deformation.

As shown in Eqs. (4), (6), and (12), the Young's moduli of the rubber tube and extensible cloth can be easily calculated using the following equation:

$$\frac{p\pi d^2}{4} = (1+k)(E_1+E_2)\frac{\pi d^2 L_0}{D}. \quad \ldots \quad (13)$$

Finally, we obtain the following equation, comprising E_1 and E_2, which can be used in the following analysis.

$$(1+k)(E_1+E_2) = \frac{pD}{4L_0}. \quad \ldots \quad (14)$$

4.2. Deformation with Load

After analyzing the pressurized situation of the actuator, we analyzed the model when a traction force was applied to the block of the actuator; it was discovered that the length x and pinch angle θ of the actuator increased, as shown in **Fig. 9**.

When the entire actuator was under different force balance states, different traction forces F under different x will reveal the relationship between the contraction force and contraction length of the actuator. In this case, because the relative positions of σ and T do not change and the traction force F is applied at the center of the block, F generates no torque on the block, and the torque balance in Eq. (6) still exists.

In this condition, the circumferential tension will eliminate each other in all directions instead of a force balance. Owing to the traction force F and pinch angle θ, the force balance equation at the end of actuator obtained using Eq. (6) is as follows:

$$F + p\frac{\pi d^2}{4}\sin\theta = (\sigma+T)\sin\theta = (1+k)(E_1+E_2)\Delta S\sin\theta. \quad (15)$$

Subsequently, from Eq. (14), we obtain

$$F = \left(\frac{pD}{4L_0}\Delta S - p\frac{\pi d^2}{4}\right)\sin\theta. \quad \ldots \quad (16)$$

Because the Young's modulus only depends on the materials, it will not change; therefore, we only need to obtain the area change ΔS and pinch angle θ. To calculate ΔS, we should visualize spreading the helix to a plane, as shown in **Fig. 10**. Because the inner length of the tube is still constrained by the wire inside, the inner length remains as L_0 (as in the initial condition), which can be calculated using Eq. (7), and $\sin\theta$ can be calculated in this triangle. For the outer length L, although we spread it along its coiled direction because it is longer than L_0, we must obtain another triangle relation for it.

Considering that θ tends to 0, the current length L should be the same as condition A, which is described

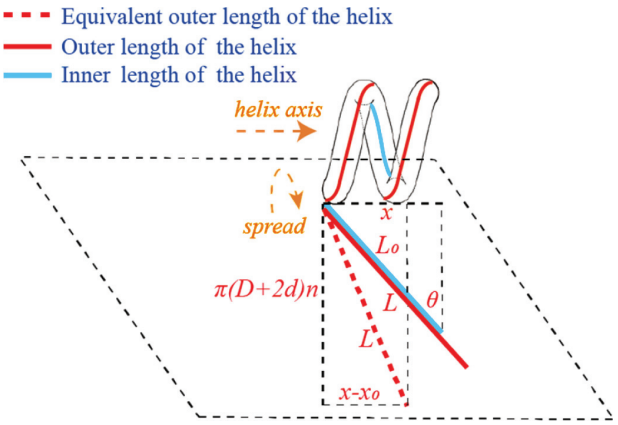

Fig. 10. By spreading the coiled actuator to a plain, we can calculate the current length L and pinch angle θ based on two triangles.

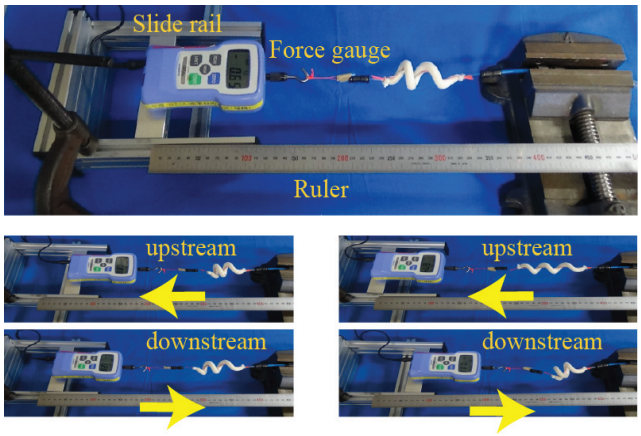

Fig. 11. Main test device and experimental method.

by Eq. (8), and the length of the actuator should be x_0. Therefore, when θ is an acute angle, the corresponding vertical length of current L should be $\pi(D+2d)n$, and the corresponding horizontal length should be $x-x_0$. Based on **Fig. 10**, we can obtain the current outer length L in a triangle, as follows:

$$\left(\pi(D+2d)n\right)^2+(x-x_0)^2=L^2. \quad \ldots\ldots\ldots (17)$$

Subsequently, from Eqs. (7) and (17), we can obtain the outer length L as follows:

$$L=\sqrt{(x-x_0)^2+\left(1+\frac{2d}{D}\right)^2 {L_0}^2}. \quad \ldots\ldots (18)$$

Using Eq. (10), we can obtain the small area as follows:

$$dS=\frac{\pi d}{4}\left(1+\frac{\sqrt{(x-x_0)^2+\left(1+\frac{2d}{D}\right)^2 {L_0}^2}}{L_0}\right)dl. \quad (19)$$

Using Eqs. (11) and (12), we can obtain the area change of the tube:

$$\begin{aligned}\Delta S &= \int_0^{L_0} 2\,dS - S_0 \\ &= \frac{\pi d}{2}\left(\sqrt{(x-x_0)^2+\left(1+\frac{2d}{D}\right)^2 {L_0}^2}-L_0\right). \quad (20)\end{aligned}$$

Finally, using Eqs. (16) and (20), we can obtain the relationship between the contraction force and current length as follows:

$$F=\left(\frac{\pi pDd}{8L_0}\left(\sqrt{\left(x-\frac{L_0 d}{\pi D}\right)^2+\left(1+\frac{2d}{D}\right)^2 {L_0}^2}-L_0\right)-p\frac{\pi d^2}{4}\right)\frac{x}{L_0}. \quad (21)$$

Table 1. Young's modulus of materials used in helical actuator.

Materials	One-way extensible cloth		Inextensible wire	Rubber tube
	Inextensible direction	Extensible direction		
Young's modulus	5.74 MPa	0.195 MPa	25.5 MPa	1.36 MPa

5. Experiments

5.1. Hysteresis

We investigated the relationship between the force and contraction length of the proposed actuator; we analyzed whether the characteristics changed based on the movement direction.

The experimental setup is shown in **Fig. 11**. The Young's moduli of the materials used in the helical actuator are shown in **Table 1**. The actuator was first pressurized to deform into a helical shape. While it was fixed at one end, the air pressure was fixed constant until the end of the experiment. On the other end, a force gauge was connected to the actuator to obtain the traction force. A ruler was placed along the moving direction to record the instant length of the actuator.

We define the movement of the force gauge in the pulling direction as upstream, and that in the opposite direction as downstream. Every traction experiment was conducted twice.

In our experiment, we discovered that hysteresis existed when we moved the force along opposite directions, as shown in **Fig. 12**, where an actuator with an outer diameter of 3 mm was pressurized under a 0.3 MPa air pressure. We discovered that in the same position, the force data in the upstream direction were always larger than those downstream.

This phenomenon is attributable to two reasons. One was hysteresis due to the viscoelastic properties of the rubber inside the actuator. In other words, the energy accumulated when the force was increased on the upstream side was dissipated as thermal energy on the downstream

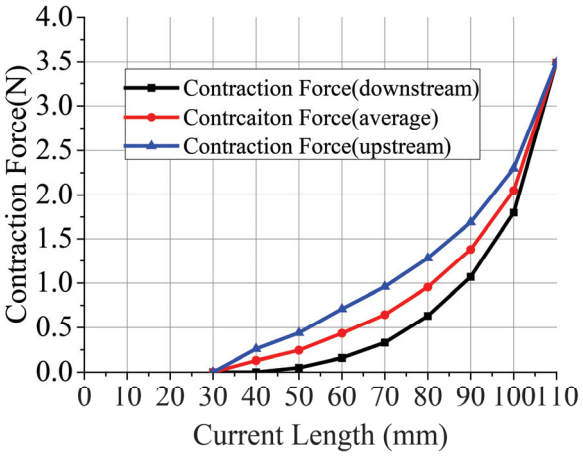

Fig. 12. Example of hysteresis in the experiments (0.3 MPa; outer diameter = 3 mm); average force was used as the true value in data analysis.

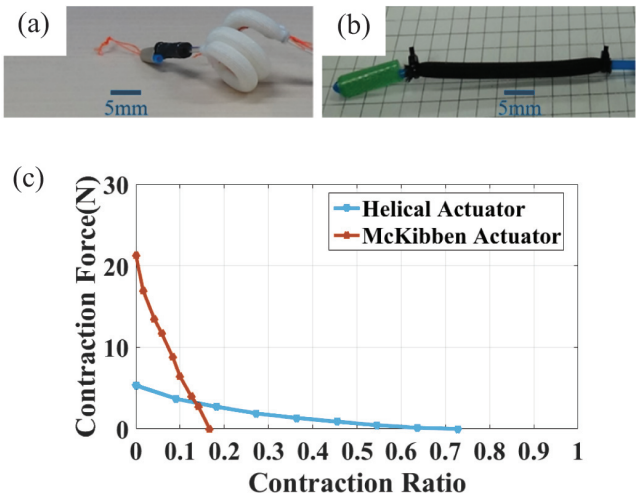

Fig. 13. (a) Helical actuator with 3 mm outer diameter contracts under 0.4 MPa. (b) McKibben actuator with 3 mm outer diameter contracts under 0.4 MPa. (c) Mckibben actuator and helical actuator of the same size compared under the same pressure.

side owing to the viscosity of the rubber. Therefore, we assumed that the force decreased even with the same displacement. The other reason was that the anisotropic cloth was deformed with respect to the rubber in the direction where the strain accumulated on the upstream side and returned to the direction that eliminated the strain on the downstream side.

5.2. Comparison with the McKibben Actuator

We compared the characteristics of the helical actuators with those of the McKibben artificial muscle, which is widely used as a contraction actuator, under the same conditions. We investigated their contraction abilities by their contraction forces under different contraction ratios. The contraction ratio was used to eliminate the effects caused by different lengths of these actuators, which can be calculated using the following equation:

$$Contraction\ ratio = \frac{Initial\ length - Current\ length}{Inital\ length}. \quad (22)$$

Here, the initial length is defined as the length of each actuator with no pressure and no load. After pressurizing the actuators to contract them, the current length was measured, whereas the traction force was increased gradually. The McKibben actuator used in this experiment was made of a flexible but inextensible braided nylon mesh shell and the same rubber tube material as that used for the helical actuator inside it. All the experiments were conducted under a 0.4 MPa air pressure; the outer diameter and initial length of both actuators were the same, i.e., 3 and 100 mm, respectively. The two actuators used in this study are shown in **Figs. 13(a)** and **(b)**. The results of the comparison between them are shown in **Fig. 13(c)**.

The maximum contraction ratio of the McKibben actuator was 0.17 with no load. As the contraction force increased, the actuator lengthened and the contraction ratio decreased. The maximum contraction force was 21.4 N when the McKibben actuator lengthened to its initial length. By contrast, the helical actuator achieved a contraction of 0.72 with no load and a maximum contraction force of 5.3 N.

These experimental results indicate that the proposed helical actuator had a much larger contraction ratio, which was over four times larger than that of the McKibben actuator. Meanwhile, the maximum contraction force of the helical actuator was approximately one-fourth that of the McKibben artificial muscle.

The McKibben actuator translates radial expansion into axial contraction to produce a contraction motion. Its conversion rate depends on the diamond shape of the mesh covering the tube surface. When the contraction ratio is low, a large contraction force is generated because the rhombus has an axially collapsed shape and the conversion ratio is high. However, as the contraction rate increases, the rhombus becomes open and its conversion rate decreases, thereby decreasing the contraction force.

Meanwhile, the proposed helical actuator generates a contraction motion based on the difference in the elongation rates of the left and right materials in the axial direction. Moreover, the expansion rate tends to be almost constant regardless of the contraction rate in the axial direction. Therefore, it exhibits the characteristics shown in **Fig. 13(c)**, unlike those of the McKibben artificial muscle.

The response speeds of this actuator and the McKibben artificial muscle were compared. In general, because the relationship power = force × speed is satisfied, when the power is constant, the displacement speed of this actuator is faster in the region where the McKibben-type artificial muscle has a larger force. Furthermore, compared with the McKibben artificial muscle, this helical actuator is designed particularly to increase the displacement rate; therefore, the displacement will change when the same external force is applied, resulting in low rigidity.

Table 2. Tube parameters used in theoretical calculation in two groups.

1st group of experiments		2nd group of experiments	
L_0: initial length	100 mm	L_0: initial length	220 mm
D: outer diameter	3.0 mm	D: outer diameter	11.6 mm
d: inner diameter	2.1 mm	d: inner diameter	8.0 mm

5.3. Validation of Mathematical Model

We analyzed our mathematical model to verify if the estimation value of the contraction force and the corresponding actuator length matched with the experimental values.

Based on the different outer diameters of the tubes, two groups of experiments were conducted. The tube parameters required for the theoretical calculations and experiments are shown in **Table 2**.

The first group was conducted using an actuator with a 3 mm outer diameter under air pressures of 0.3 and 0.4 MPa. The same traction tests were conducted four times. The results of this group are shown in **Fig. 14**, where the average values are used to draw a line, and errors are shown using an error bar.

The second group of experiments was conducted on an actuator with a 11.6 mm outer diameter under air pressures of 0.2 and 0.3 MPa. The same experiments were conducted four times, and the data processing method was the same as that of the first group. The results are shown in **Fig. 15**.

As shown by the results, the contraction force generated by the helical actuator was positively correlated with the contraction length, air pressure, and outer diameter of the rubber tube. Except for the experiment on the actuator with an 11.6 mm outer diameter under 0.3 MPa, the mathematical model proved that the theoretical estimation value generally fitted well with the real value under different pressures and different actuator sizes. Meanwhile, under 0.3 MPa, the helical actuator with an 11.6 mm outer diameter generated a larger contraction force compared with the theoretical value. This is attributable to the following reason: in this model, only the two directions shown in **Table 1** were considered as the characteristics of the one-way extensible cloth covering the tube. However, in reality, as the pressure increases, the thread that sewed the cloth will be stretched, resulting in a larger than expected cross-sectional area of the tube.

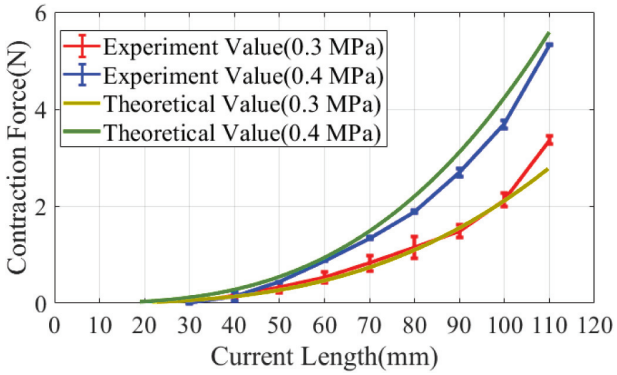

Fig. 14. Contraction experiments on actuator with 3 mm outer diameter under 0.3 and 0.4 MPa air pressures.

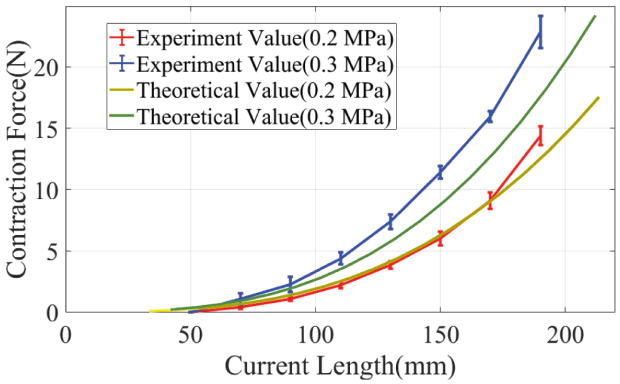

Fig. 15. Contraction experiments on actuator with 11.6 mm outer diameter under 0.2 and 0.3 MPa air pressures.

6. Discussion

Because the proposed actuator has a soft structure and can generate a large displacement, it can be applied to assist in the joint motion of the human body. To illustrate, its effectiveness when applied to assist the ankle joint motion is analyzed in the following.

The dorsiflexion movement of the ankle joint promotes blood flow in the deep vein and is effective for the prevention of economy-class syndrome. For elderly people who tend to remain in bed for long periods of time, flexible devices capable of moving their ankles automatically are highly demanded. This operation requires a traction force of approximately 20 to 30 N in the operating range of approximately 40° from the plantar flexion to dorsiflexion [22].

Figure 16 shows the behavior of a helical actuator mounted on the shin of an ankle model with human-like characteristics. In this experiment, the wire in the tube was replaced by a non-stretch fabric to strengthen the structure. The specifications of the actuator were an inner diameter of 8 mm, an outer diameter of 11 mm, and a length of 300 mm. When an air pressure of 0.3 MPa was applied, the contraction ratio was 0.4, and the ankle joint can be actively rotated by approximately 30°. In addition, it was confirmed that the movable range was approximately 1.5 times larger than that of a McKibben artificial muscle of the same size. To rotate approximately 40° further, a helical actuator with an inner diameter of approximately 14 mm or four sets in parallel are required. The speed of the actuator for supporting dorsiflexion can be adjusted by adjusting the flow rate of air supplied to the actuator. Specifically, the speed can be adjusted by having variable valve opening area of the speed controller.

Using a soft pneumatic helical actuator for such an op-

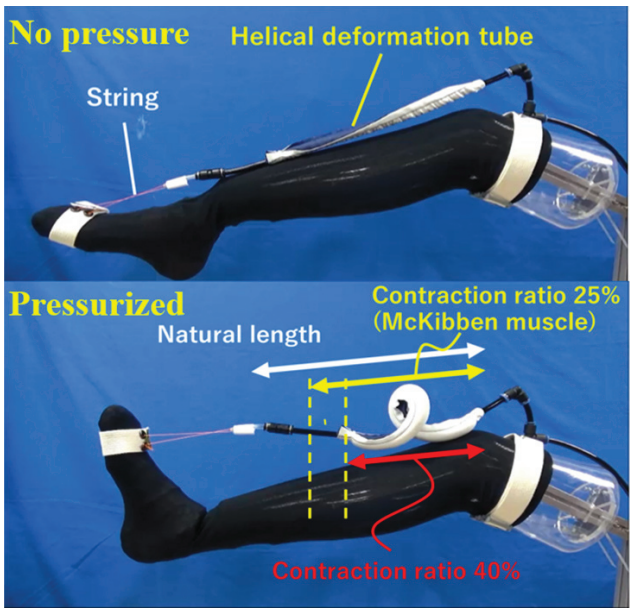

Fig. 16. Helical actuator can effectively assist ankle joint motion.

eration support offers the following two advantages: i) because the contracting actuator does not comprise local swelling or bending parts, pain will not be inflicted to the human body even if it is in contact with the human skin; ii) because it can be arranged to pull in a direction perpendicular to the foot, no undue load is exerted on the joints.

7. Conclusion

We proposed a soft actuator that generates a high contraction ratio by deforming helically under an air pressure. The proposed actuator has a simple structure and can be easily fabricated by fixing a one-way extensible cloth, rubber tube, and non-stretchable wire together. Furthermore, we derived a mathematical model that illustrated the characteristics of this actuator and clarified the relationship between the contraction force and length of the actuator. Compared with the McKibben actuator, the contraction force of the proposed helical actuator was approximately $1/4$ less, but the contraction rate was four times larger; hence, it is applicable to wearable actuators that support human joint movements.

In the future, we will further investigate methods to derive the optimum design parameters based on the operation purpose. In particular, we plan to investigate the effect of the fiber angle of a one-way extensible cloth on the stretch ratio and force using an advanced mathematical model. Additionally, we plan to build a model that considers dynamic effects.

References:

[1] C. Laschi, B. Mazzolai, and M. Cianchetti, "Soft robotics: Technologies and systems pushing the boundaries of robot abilities," Science Robotics, Vol.1, No.1, eaah3690, 2016.

[2] D. Rus and M. T. Tolley, "Design fabrication and control of soft robots," Nature, Vol.521, pp. 467-475, 2015.

[3] T. Noritsugu, M. Takaiwa, and D. Sasaki, "Development of power assist wear using pneumatic rubber artificial muscles," J. Robot. Mechatron., Vol.21, No.5, pp. 607-613, 2009.

[4] C. Thakur, K. Ogawa, and Y. Kurita, "Active passive nature of assistive wearable gait augment suit for enhanced mobility," J. Robot. Mechatron., Vol.30, No.5, pp. 717-728, 2018.

[5] T. Kosaki and S. Li, "A Water-Hydraulic Upper-Limb Assistive Exoskeleton System with Displacement Estimation," J. Robot. Mechatron., Vol.32, No.1, pp. 149-156, 2020.

[6] L. N. Awad et al., "A soft robotic exosuit improves walking in patients after stroke," Sci. Transl. Med., Vol.9, No.400, eaai9084, 2017.

[7] P. Polygerinos et al., "Soft robotic glove for hand rehabilitation and task specific training," 2015 IEEE Int. Conf. on Robotics and Automation (ICRA), pp. 2913-2919, 2015.

[8] H. Al-Fahaam, S. Davis, and S. Nefti-Meziani, "Wrist rehabilitation exoskeleton robot based on pneumatic soft actuators," 2016 Int. Conf. for Students on Applied Engineering (ICSAE), pp. 491-496, 2016.

[9] T. Kawamura, H. Kawahara, and M. Nakazawa, "Control of Vertebrate Backbone System by Using Artificial Rubber Muscles," J. Robot. Mechatron., Vol.7, No.6, pp. 483-487, 1995.

[10] S. Krishna, T. Nagarajan, and A. M. A. Rani, "Review of current development of pneumatic artificial muscle," J. of Applied Sciences, Vol.11, No.10, pp. 1749-1755, 2011.

[11] B. Tondu and P. Lopez, "Modeling and control of McKibben artificial muscle robot actuators," IEEE Control Systems Magazine, Vol.20, No.2, pp. 15-38, 2000.

[12] N. S. Usevitch, A. M. Okamura, and E. W. Hawkes, "APAM: antagonistic pneumatic artificial muscle," 2018 IEEE Int. Conf. on Robotics and Automation (ICRA), pp. 1539-1546, 2018.

[13] W. Felt, M. A. Robertson, and J. Paik, "Modeling vacuum bellows soft pneumatic actuators with optimal mechanical performance," 2018 IEEE Int. Conf. on Soft Robotics (RoboSoft), pp. 534-540, 2018.

[14] E. R. Perez-Guagnelli, S. Nejus, J. Yu et al., "Axially and radially expandable modular helical soft actuator for robotic implantables," IEEE Int. Conf. on Robotics and Automation (ICRA), pp. 4297-4304, 2018.

[15] L. H. Blumenschein et al., "A tip-extending soft robot enables reconfigurable and deployable antennas," IEEE Robotics and Automation Letters, Vol.3, No.2, pp. 949-956, 2018.

[16] L. H. Blumenschein et al., "Helical actuation on a soft inflated robot body," 2018 IEEE Int. Conf. on Soft Robotics (RoboSoft), pp. 245-252, 2018.

[17] R. Geer and S. Li, "Examining the coiling motion of soft actuators reinforced with tilted helix fibers," American Society of Mechanical Engineers (ASME) 2018 Conf. on Smart Materials, Adaptive Structures and Intelligent Systems, Paper No.SMASIS2018-8038, 2018.

[18] P. Yuan, G. Kawano, and H. Tsukagoshi, "Soft Pneumatic Helical Actuator with High Contraction Ratio," 2019 IEEE/RSJ Int. Conf. on Intelligent Robots and Systems (IROS), pp. 8300-8305, 2019.

[19] F. Connolly et al., "Mechanical programming of soft actuators by varying fiber angle," Soft Robotics, Vol.2, No.1, pp. 26-32, 2015.

[20] R. Mutlu, G. Alici, and W. Li, "Three-dimensional kinematic modeling of helix-forming lamina-emergent soft smart actuators based on electroactive polymers," IEEE Trans. on Systems, Man, and Cybernetics: Systems, Vol.47, No.9, pp. 2562-2573, 2017.

[21] K. Han, N. H. Kim, and D. Shin, "A novel soft pneumatic artificial muscle with high-contraction ratio," Soft Robotics, Vol.5, No.5, pp. 554-566, 2018.

[22] R. N. Stauffer, E. Y. Chao, and R. C. Brewster, "Force and motion analysis of the normal, diseased, and prosthetic ankle joint," Clinical Orthopaedics and Related Research, Vol.127, pp. 189-196, 1977.

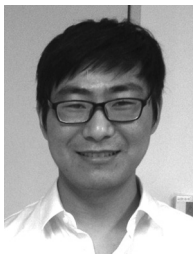

Name:
Peizheng Yuan

Affiliation:
Tokyo Institute of Technology

Address:
2-12-1 Ookayama, Meguro-ku, Tokyo 152-8552, Japan

Brief Biographical History:
2020 Master's degree in Engineering, Tokyo Institute of Technology
2020- Ph.D. Candidate

Main Works:
• P. Yuan, G. Kawano, and H. Tsukagoshi, "Soft Pneumatic Helical Actuator with High Contraction Ratio," 2019 IEEE/RSJ Int. Conf. on Intelligent Robots and Systems (IROS), pp. 8300-8305, 2019.

Name:
Ginjiro Kawano

Affiliation:
Tokyo Institute of Technology

Address:
2-12-1 Ookayama, Meguro-ku, Tokyo 152-8552, Japan

Brief Biographical History:
2018 Master's degree in Engineering, Tokyo Institute of Technology
2018- NIPPON STEEL CORPORATION

Main Works:
• Fluid powered actuator

Name:
Hideyuki Tsukagoshi

Affiliation:
Tokyo Institute of Technology

Address:
2-12-1 Ookayama, Meguro-ku, Tokyo 152-8552, Japan

Brief Biographical History:
1994 Master's degree in Engineering, Tokyo Institute of Technology
1998 Doctor's degree in Engineering, Tokyo Institute of Technology
1998-2004 Research Associate, Tokyo Institute of Technology
2004- Associate Professor, Tokyo Institute of Technology

Main Works:
• H. Tsukagoshi, K. Fuchigami, E. Watari, and A. Kitagawa, "Deformable Anchor Ball for Thrown Referring to Octopus Suckers," J. Robot. Mechatron., Vol.26, No.4, pp. 477-485, 2014.

Membership in Academic Societies:
• The Institute of Electrical and Electronics Engineers (IEEE) Robotics and Automation Society
• The Robotics Society of Japan (RSJ)
• The Japan Society of Mechanical Engineers (JSME)
• The Japan Fluid Power System Society (JFPS)